Icarus 204 (2009) 103–113

Contents lists available at ScienceDirect

Icarus

journal homepage: www.elsevier.com/locate/icarus

North polar frontal clouds and dust storms on Mars during spring and summer

Huiqun Wang [a,*], Jenny A. Fisher [b]

[a] Harvard-Smithsonian Center for Astrophysics, 60 Garden St., Cambridge, MA 02138, USA
[b] School of Engineering and Applied Sciences, Harvard University, 29 Oxford St., Cambridge, MA 02138, USA

ARTICLE INFO

Article history:
Received 28 October 2008
Revised 16 April 2009
Accepted 30 May 2009
Available online 13 June 2009

Keyword:
Mars

ABSTRACT

The complete archive of Mars Global Surveyor (MGS) Mars Orbiter Camera (MOC) Mars Daily Global Maps (MDGM) are used to study north polar clouds and dust storms that exhibit frontal structures during the spring and summer (L_s 0–180°). Results show that frontal events generally follow the edge of the polar cap during spring and mid/late summer with a gap in the distribution in early summer. The exact duration and timing of the gap vary from year to year. Ten to twenty percent of spring and summer time frontal events exhibit complex morphologies. Distinct temperature signatures are associated with features observed in images in many but not all cases. The general travel paths of the frontal events are eastward around the polar cap. Westward paths exist only at the edge of the polar cap in late spring/early summer. Occasionally, the paths curve toward or away from the polar cap in certain longitude sectors.

1. Introduction

Clouds and dust storms are important components of the martian climate system and are closely related to the martian atmospheric circulation. The Mars Global Surveyor (MGS) has greatly advanced our knowledge of these features through systematic daily global observations (Albee, 2002). MGS was in a 2AM–2PM Sun synchronous orbit. MGS Mars Orbiter Camera (MOC) (Malin et al., 1992) took a red–blue pair of limb-to-limb global map swaths at 7.5 or 3.75 km/pixel resolution on each orbit during March 1999–October 2006. Mars Daily Global Maps (MDGM) composed of 13 consecutive pairs of global map swaths each (Wang and Ingersoll, 2002; Cantor, 2007) provide an invaluable dataset for studying clouds and dust storms. In addition, MGS Thermal Emission Spectrometer (TES) (Christensen et al., 1992) made concurrent observations of atmospheric temperatures, dust/ice opacities, and water vapor abundances before August 2004. The general spatial and temporal distributions of clouds and dust storms have been examined using MOC or TES data (e.g., Cantor et al., 2001; Cantor, 2007; Pearl et al., 2001; Wang and Ingersoll, 2002; Smith, 2004, 2008; Tamppari et al., 2008), providing important constraints for atmospheric models (e.g., Richardson et al., 2002; Toigo et al., 2002; Hinson and Wilson, 2004; Basu et al., 2004, 2006; Rodin and Wilson, 2006). A few studies have focused on special cloud/dust storm types, such as orographic clouds and spiral dust storms over major volcanoes (Rafkin et al., 2002; Benson et al., 2003, 2006), and dust storms whose morphologies are analogous to fronts in terrestrial cyclones (called "frontal dust storms") (James et al., 1999; Wang et al., 2003, 2005; Wang, 2007).

Previous studies of frontal dust storms concentrated on northern fall and winter (L_s 180–360°, solar longitude L_s is an angular measure of season with 0° at the northern spring equinox, 90° at the summer solstice, 180° at the fall equinox and 270° at the winter solstice). Martian climate responds to solar insolation much faster than Earth climate. The hottest time period at northern high latitudes on Mars is around L_s 90° and the coldest is around L_s 270°. However, there is currently no climate-based definition for martian season. We therefore define martian season the same way as we do for Earth in this paper. As a result, these terms are not for describing the corresponding atmospheric conditions.

The fall and winter frontal events usually exhibit simple curvilinear dust bands and travel eastward around the north pole. Occasionally, they get entrained in the lower branch of the Hadley circulation and travel southward through low topographic channels: Acidalia, Arcadia and Utopia (called "flushing storms") (Wang et al., 2003). Frontal dust storms observed in MOC images often show anomalies in TES temperatures (Wang et al., 2005) and are probably associated with baroclinic/barotropic waves and instabilities (James et al., 1999; Wang et al., 2005; Wilson et al., 2006; Basu et al., 2006). The classical frontal system as seen in terrestrial cyclones is usually composed of a cold front, a warm front and an occluded front at the conjunction (Houze, 1994). Martian frontal dust storms in fall and winter usually lack the expression of a warm front, and very few cases have attached cyclonic spirals (Wang et al., 2003, 2005). This is possibly due to the following

* Corresponding author.
E-mail address: hwang@cfa.harvard.edu (H. Wang).

0019-1035/$ - see front matter © 2009 Elsevier Inc. All rights reserved.
doi:10.1016/j.icarus.2009.05.028

factors: a lack of water vapor available to condense during this season and highlight the warm front, relatively weak wind strength in the warm sector that is insufficient to lift and concentrate dust, and the position of the occlusion being on the seasonal polar cap in polar night. Frontal dust storms are frequently observed in mid-fall and mid-winter and are suppressed at the winter solstice (L_s 270°). This pattern is coincident with eastward traveling zonal wave number $m = 3$ waves with periods of 2–3 sols (martian solar day), indicating the involvement of this wave mode in frontal dust storms (Wang et al., 2005; Basu et al., 2006; Hinson, 2006). The development from frontal dust storms to flushing dust storms also suggests the role of this wave mode (Wang et al., 2003; Wilson et al., 2006). The most commonly observed traveling waves in the first scale height of the martian atmosphere (bottom 10 km) are eastward traveling $m = 1$–3 waves (periods of 2–8 sols) with mixed barotropic/baroclinic character (Barnes, 1980, 1981; Barnes et al., 1993; Banfield et al., 2004; Hinson, 2006). GCM simulations show reduction of traveling waves near the winter solstice and suggest that this behavior is due to the stabilization of the jet and associated weakening of wave excitation (Barnes et al., 1993; Basu et al., 2006; Kuroda et al., 2007). Note that upper level (e.g., 0.5 mb) wave activity is strongest during the solstice period, and is dominated by zonal wave $m = 1$.

This paper concentrates on northern spring and summer time (L_s 0–90–180°) to complete the catalog of north polar frontal events observed by MGS (Wang et al., 2005; Wang, 2007). Although the circulations in late summer (L_s 150–180°) and early spring (L_s 0–30°) are in some degree winter-like (Banfield et al., 2003, 2004; Tyler and Barnes, 2005; Basu et al., 2006), we have included clouds and dust storms in these periods for continuity with previous studies. Clouds are abundant in spring and summer (L_s 0–90°), and local and regional dust storms also occur (Cantor et al., 2001; Wang and Ingersoll, 2002; Smith, 2004, 2008; Tamppari et al., 2008). We have studied both clouds and dust storms that exhibited front-like morphologies in the north polar region (45–90°N). In the absence of polar night, consecutive MOC images have large overlap at high latitudes. As a result, the two-hourly developments of some relatively large clouds/dust storms are recorded. Prominent traveling and stationary waves in early spring and late summer can affect the polar energy budget and the transport of dust and water vapor (Banfield et al., 2003, 2004; Hinson, 2006). Frontal events provide a link between observables and underlying atmospheric dynamics. GCM and mesoscale simulations show circulation patterns consistent with the shapes and motions of clouds observed in images (e.g., Richardson et al., 2002; Newman et al., 2002b; Rafkin et al., 2002; Toigo et al., 2002; Montmessin et al., 2004; Tyler and Barnes, 2005; Wilson et al., 2006; Basu et al., 2006; Kauhanen et al., 2008). Our study will add to the observations with which models can be compared for explanation, validation and improvement.

2. Data analysis approach

2.1. Morphology

The spring and summer frontal clouds and dust storms observed in MDGM range from a few hundred to a few thousand kilometers and exhibit a wide variety of morphologies. Martian dust storms are conventionally classified as "local" (long axis <2000 km; area $<1.6 \times 10^6$ km^2 or duration < 3 sols), "regional" (long axis > 2000 km; area > 1.6×10^6 km^2 and duration > 3 sols) or "planet-encircling"/"global" dust storms (Zurek and Martin, 1993; Cantor, 2007). Only local and regional storms are relevant to this study. In dynamical meteorology, atmospheric circulations are usually classified as "local" (kilometer), "meso" (tens to hundreds of kilometers), "synoptic" (hundreds to thousands of kilometers), or "planetary" (tens of thousands of kilometers) scale circulations (Holton, 1992). The terminologies for dust storms and circulations are related. Local dust storms and clouds are presumably influenced by local and mesoscale circulations such as convection and orographic flows, while regional dust storms and clouds are probably related to synoptic cyclogenesis and planetary waves. Due to the small radius of Mars, the planetary and synoptic scales are not well separated – the wavelengths of the largest planetary waves (with zonal wave number $m < 4$) approach synoptic scale, which is comparable to the size of a regional dust storm. Consequently, planetary circulation can substantially influence the development of a regional storm and vice versa.

Fig. 1 shows examples of the most commonly observed types of frontal events in spring and summer. In addition to simple curvilinear fronts (Fig. 1a), there are cases with substantial curvatures (arc, Fig. 1b and c), wavy fronts (Fig. 1d and e), commas (Figs. 1j–l and 5), λ shapes (Fig. 1m and n), tightly wrapped spirals (Fig. 1h), and spirals with 2–3 arms (Figs. 1f, i, n, and o and 6). These images represent different developmental histories of frontal events and indicate the role of vorticity in shaping clouds and dust storms. Terrestrial comma-shaped clouds are usually associated with synoptic scale (thousands of kilometers) cyclones in midlatitudes or mesoscale (hundreds of kilometers) lows in polar regions (Houze, 1994). Martian commas also range from hundreds to thousands of kilometers in length, but are usually made visible by dust (sometimes in combination with cloud). In addition to the usual north–south orientation (Fig. 1j), martian commas sometimes appear upside-down (Fig. 5) or sideways (Fig. 1k and l) in projected images, but they all show cyclonic rotation. The comma in Fig. 5 developed into the tightly wrapped spiral in Fig. 1h within one sol. Another way to form a spiral is indicated in panels d–f of Fig. 1. Although these are unrelated events, the images suggest that developing waves along a front can create a spiral with two arms. Alternatively, a spiral can develop at the end of a wavy front instead of at the center (Fig. 1g). Separate fronts can rotate around a common center to form a multi-armed spiral (Figs. 6 and 1i). Fig. 1m shows a complex frontal system with two dust arms in a λ configuration. Fig. 1o shows two dust arms (the eastern one was covered by cloud) connected by a spiral to the north, analogous to typical frontal systems (cold, warm and occluded front) in terrestrial cyclogenesis (Wang and Ingersoll, 2002). Fig. 1n shows an example similar to Fig. 1o, but the event is composed purely of ice clouds.

Arcs in MDGM can be composed of dust and/or ice. They vary from a few hundred to a few thousand kilometers and can have openings in any direction (Fig. 1b–e). Cantor et al. (2002) reported repeated arc-shaped clouds during L_s 124–140° over three Mars years. Occasionally, an arc can develop into a spiral feature (Fig. 1o). Hubble Space Telescope previously observed a tightly wrapped ice cloud in the same longitudinal sector and season (image ID: PIA01545). Arcs appear to be characteristic of ice clouds in the 45–135°W sector (north of Tharsis) in mid-summer. They reflect rotational circulations associated with shear or curvature. Mesoscale simulations show strong transient eddies in the region between Tharsis and the polar cap around L_s 135° that can potentially create the arc-shaped clouds observed in images (Tyler and Barnes, 2005). Strong wind excursions associated with cap edge katabatic flow or planetary waves can produce arc-shaped surface wind stress patterns suggestive of dust arcs at the polar cap edge (Tyler and Barnes, 2005; Kauhanen et al., 2008).

Amorphous ice clouds are a major component of the polar hood. Diffuse dust haze is also a contributor to the polar hood in late summer. Since they reflect general large-scale atmospheric conditions (temperature and mean winds) rather than dynamical instabilities and local to synoptic scale circulations, we do not include them in our analysis. However, they contribute to optical depths.

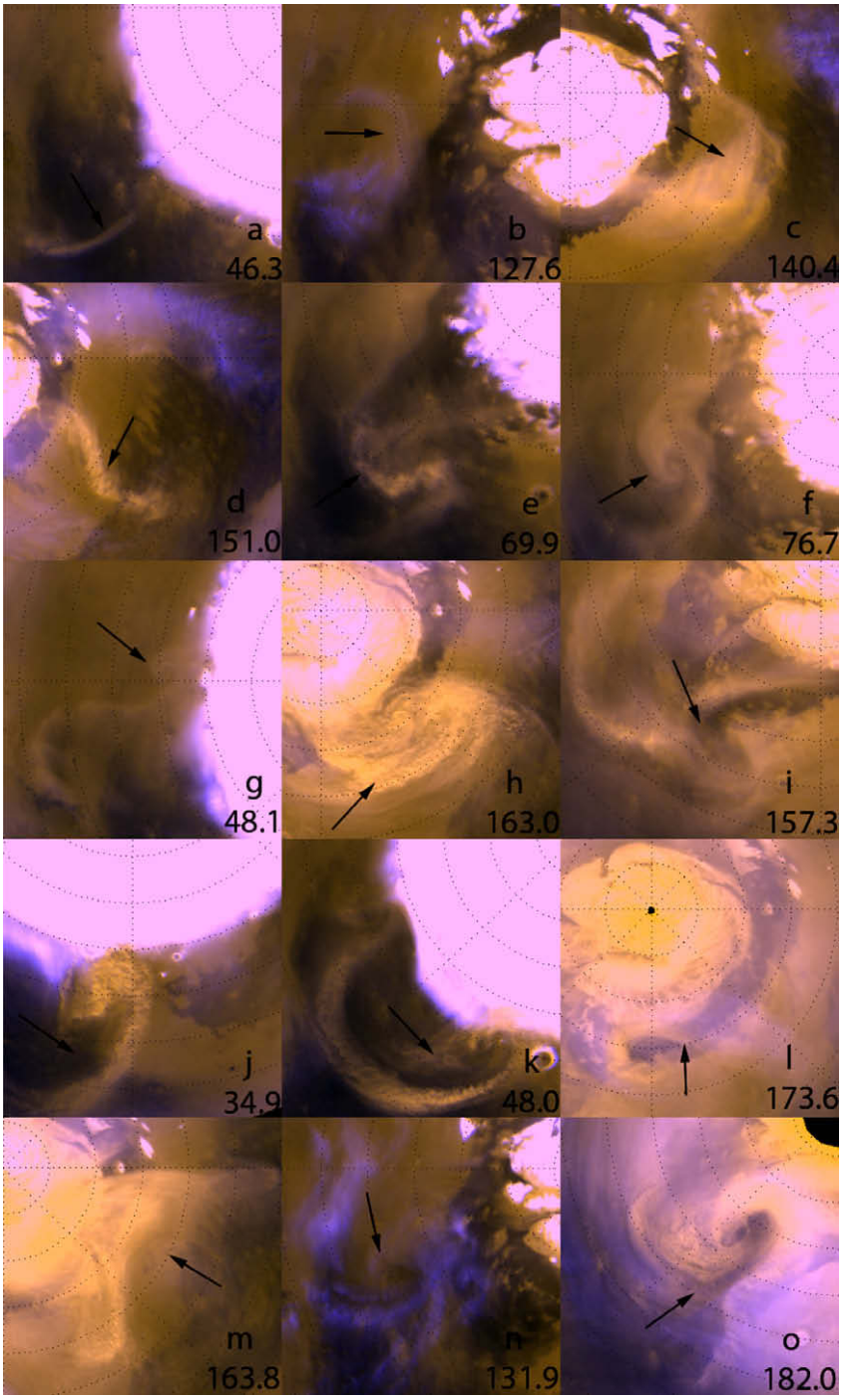

Fig. 1. Examples of north polar frontal events observed in spring and summer. Images are in polar stereographic projection, with 0° longitude oriented downwards. Dust storms appear yellow and clouds appear blue. L_s is indicated in each panel. Panels h, l, m, and o are from Mars Year 24; panels b, e, f, j and k are from Mars Year 25; panels a, c, d, g and i are from Mars Year 26; and panel n is from Mars Year 27. (a) Simple front (b) cloud arc (c) dust arc (d and e) wavy front (f) spiral in the middle (g) spiral on the end (h) spiral (i) spiral with three arms (j–l) comma (m) λ-shape (n) λ composed purely of clouds (o) classical occlusion. (For interpretation of the references to color in this figure legend, the reader is referred to the web version of this article.)

Using TES data, Tamppari et al. (2008) found high dust and water ice optical depths before L_s 75° and after L_s 165°. According to MDGM, a substantial fraction of the opacity should have come from amorphous cloud / dust haze in the polar hood. Although the polar hood as a single entity is not counted, dust storms and clouds embedded in the polar hood are included as long as they exhibit front-like structure.

TES opacity retrievals show low ice optical depths and high dust optical depths at northern high latitudes (60–90°N, especially in the 0–90°W quadrant) in late spring and early summer (Tamppari et al., 2008). Individual MGS global map swaths are able to show both the 2PM and 2AM sides of the polar cap near the summer solstice (this is not possible in other time periods due to illumination limitations). The 2PM side appears clear but the 2AM side appears dusty and cloudy. Since pixels on the 2AM side are assigned low weight, they are concealed in MDGM (Wang and Ingersoll, 2002). MDGM shows substantial dust activity in the north polar region in late spring (L_s 60–90°), consistent with TES opacity observations

(Tamppari et al., 2008). MDGM shows little dust (or ice) in early summer (L_s 90–120°), but TES (daytime) dust opacities remain high until L_s 110° in both Mars Years 25 and 26 (Tamppari et al., 2008). Some MDGMs during L_s 90–110° appear to be dust storm free, but the corresponding TES tracks show high dust opacities (not shown). The discrepancy between TES and MOC observations is probably due to the presence of translucent dust haze (without clear boundary) that is not apparent in MOC images. Such a dust haze may be supplied by dust devils since dust devils are usually smaller than the resolution of the global map swath and can maintain a background haze through dust lifting in convective vortices (Newman et al., 2002a; Basu et al., 2004; Greeley et al., 2003; Balme and Greeley, 2006). Dust devil track percent coverage during northern spring and summer is highest in the band between 40°N and 65°N and lowest poleward of 65°N (Whelley and Greeley, 2008). This is at odds with the assumption that dust devils provide the haze observed by TES but not MOC. However, dust devils are not always associated with tracks on the surface (Fisher et al., 2005). The possibility is therefore not ruled out. Alternatively, dust advected from the night side or raised by small scale circulation at the edge of the residual cap can also make a dust haze.

Orographic clouds are not accounted for in this study, neither. In the domain of interest (45–90°N), they are mainly located on the northern slopes of Tharsis (from Alba Fossae to Tempe Fossae) and Arabia (Deuteronilus Mensae and Protonilus Mensae) and appear as patches. They occasionally move away from their original locations and adopt front-like shapes during the process. These transformed clouds may be related to topographic winds and are counted in the catalog.

2.2. MDGM frontal event catalog

The complete MGS MDGM archive (May 1999–October 2006) (Wang and Ingersoll, 2002) has been used to study north polar (45–90°N, 0.1° × 0.1°) clouds and dust storms that exhibit frontal structures, referred to as "frontal events" in this paper. This data set includes four MGS mapping years of observations and covers the spring and summer seasons of Mars Years 24–28 (Mars year convention follows Clancy et al. (2000)). The first MGS mapping year started in late summer of Mars Year 24.

We have recorded the position of each event in MDGM using a representative point judged by eye. This point is usually in the middle of a simple front/arc or at the center of a comma head/spiral, consistent with previous studies (Wang et al., 2005; Wang, 2007). Area is measured by summing the areas of dusty/cloudy pixels associated with each event in north polar MDGM (45–90°N). As a result, areas for large events near 45°N are lower limits. Composition is judged by color (red for dust, blue for ice) in MDGM. In cases when a judgment based on color alone is ambiguous, we use images from adjacent days to provide additional information. Shape is classified as simple front, arc, comma, spiral, frontal system, and other. Events that last multiple days are linked and tagged with "New" status on the first day and "Old" status on subsequent days. The final catalog contains 2422 frontal events (82% of which are "New") and is a result of examining the entire spring and summer time MDGM archive three times.

3. Results

3.1. Time–latitude distribution

Fig. 2 shows the time–latitude distribution of different sized frontal events in the north polar region during the springs and summers of Mars Years 24–28 (1999–2006). They generally follow the polar cap edge during the spring and in late summer with a hiatus in between. The overall seasonal evolution is similar among the different years. Cantor et al. (2002) compared MGS MOC images taken between 1997 and 2001. They found that some summertime clouds and dust storms recurred within a few degrees of solar longitude each year. Despite this high degree of repeatability, the timing of the hiatus can shift by up to ~10° L_s from year to year, and the duration of the hiatus can vary from ~15° to ~25° L_s (Year 25: L_s 105–123°; Year 26: L_s 91–115°; Year 27: L_s 95–111°; Year 28: L_s 99–113°).

The composition of frontal events changes with season. Frontal events in early spring and late summer usually involve both dust and ice. On one hand, cross-frontal circulation in growing baroclinic eddy can lift dust and condense ice, generating dust–ice system self consistently (Wang and Ingersoll, 2002). On the other hand, polar hood clouds can be advected by large-scale circulation to partly cover dust storms (Montmessin et al., 2004). The frontal events observed just before the early summer hiatus are predominately dust storms, and those after the hiatus are predominately ice clouds. Translucent dust haze may be present during the hiatus period, especially in the 0–90°W sector (Section 2.1), but frontal events are absent. Interannual variability in the timing and duration of the hiatus suggests corresponding variability in the timing of when surface winds fall below the dust lifting threshold and when in the season atmospheric saturation is attained. In early summer, the exposed residual polar cap supplies a large amount of water vapor to the atmosphere, but clouds (front-like or not) are absent in the polar region, suggesting a large atmospheric water vapor holding capacity due to warm temperatures (Richardson et al., 2002; Smith, 2004, 2008; Tamppari et al., 2008). TES data show no polar jet (due to weak large-scale meridional temperature gradient) and few stationary and traveling planetary waves in the polar region in early summer, which can potentially limit the occurrence of frontal dust storms (Banfield et al., 2003, 2004). Mesoscale simulations suggest that baroclinic transients occur along a summer jet and interact with katabatic flow off the polar cap (Tyler and Barnes, 2005). The summer jet results from the temperature contrast at the edge of the residual polar cap, but the strength of the jet is much weaker and the depth much shallower in summer than in winter (Tyler and Barnes, 2005). Frontal dust storms during the fall and winter also show a hiatus near the winter solstice period (Wang et al., 2003, 2005; Wang, 2007). In this case, TES data show that the polar jet is very strong (Banfield et al., 2003). GCM simulations show that the deep zonal wave $m = 1$ is very strong, but the relatively shallower zonal waves $m \geqslant 2$ are suppressed in this period (Kuroda et al., 2007; Basu et al., 2006; Wilson et al., 2006). GCM simulations also show that the eddy flux of cloud is negligible near the winter solstice (Montmessin et al., 2004).

The areas of the 2422 observed frontal events range from 740 km^2 to 1.5×10^6 km^2, with a median of 6.9×10^4 km^2. Nine hundred of the events have areas less than 5×10^4 km^2, 89 have areas greater than 5×10^5 km^2 and 11 have areas greater than 1×10^6 km^2. For a curvilinear front, an area of 5×10^5 km^2 corresponds to a long axis of 2000 km, assuming an aspect ratio of 1:8. The lifetimes of observed frontal events range from a few hours to five sols. These events are therefore local or regional according to conventional dust storm terminology (Zurek and Martin, 1993; Cantor, 2007). Large frontal events are often observed before L_s 50° and after L_s 150°. Atmospheric circulation during these periods is characterized by the presence of a winter-like polar jet and planetary waves that are important for cyclogenesis (Tyler and Barnes, 2005; Wilson et al., 2006). The late summer events appear especially impressive considering that they are larger than the polar cap (e.g., Fig. 1m). Dust storms in late spring that appear just before the hiatus are also relatively large. Although TES data indicate that the late spring polar jet and traveling waves are much

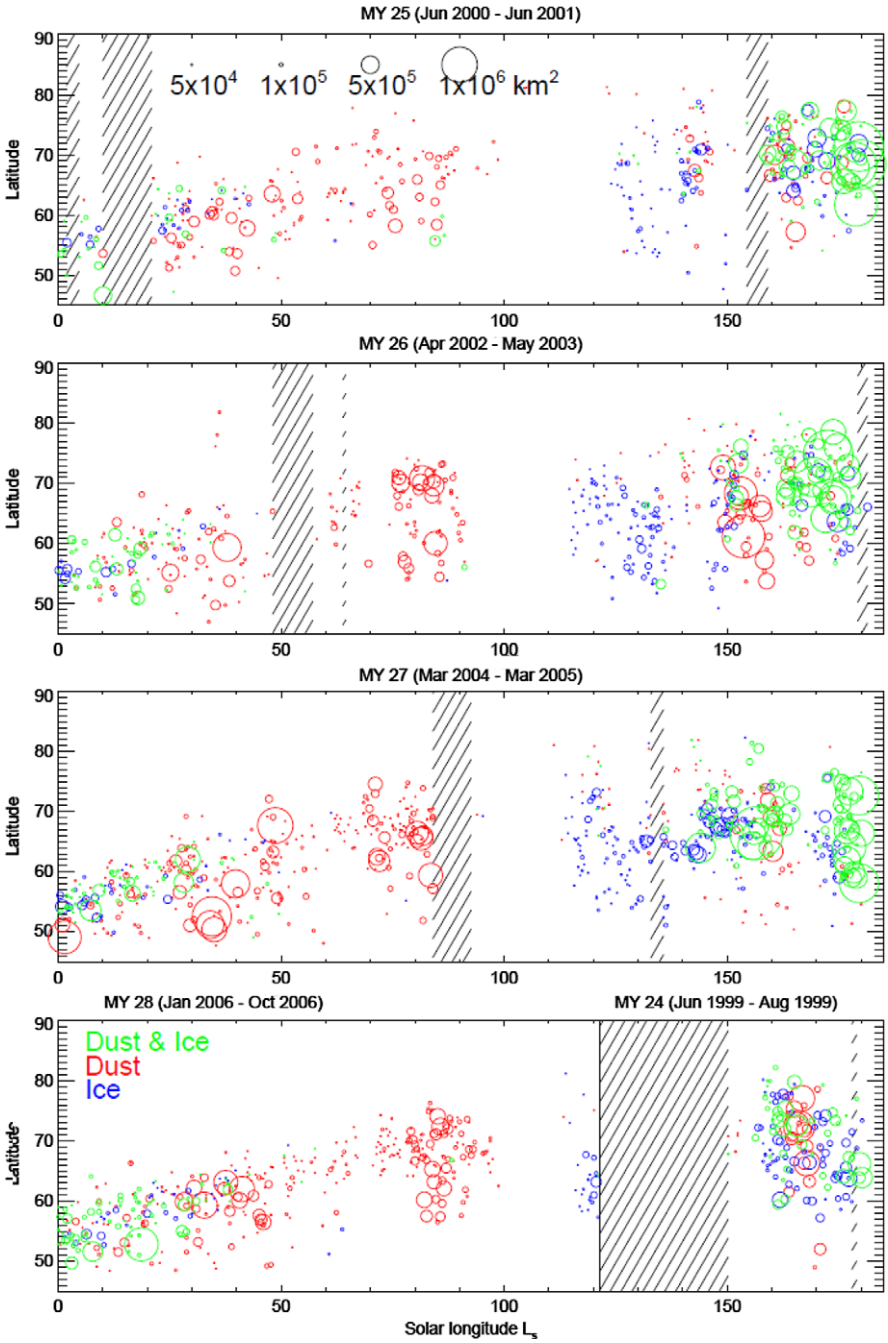

Fig. 2. Time (L_s) latitude distribution of north polar frontal events (red – dust, blue – ice, green – both dust and ice) for Mars Years 24–28 (1999–2006). The bottom panel is a combination of L_s 0–122° of Mars Year 28 and L_s 150–185° of Mars Year 24. The symbol sizes are proportional to the areas of the events. Note that the latitudinal extent of the symbols does not correspond to that of the observed storms. Events smaller than 5×10^4 km^2 are plotted with the smallest symbol size in the legend. Shaded vertical bars indicate periods with missing data. (For interpretation of the references to color in this figure legend, the reader is referred to the web version of this article.)

weaker than those early in the season (Banfield et al., 2004), mesoscale simulations show strong eddy excursion winds associated with zonal wave number $m = 2$ and prominent surface frontal structure in this period (Tyler et al., 2008). However, the simulated waves are intermittent and therefore are not necessarily expected to be evident in the TES data analysis of Banfield et al. (2004). Comparing results for different years, we find that frontal events larger than 5×10^5 km^2 occur least frequently in late summer of Mars Year 24 and spring of Mars Year 25. Although large frontal events appear to be related to planetary waves and cyclogenesis, small ones can originate from different mechanisms despite their frontal appearances. For example, cloud arcs in mid-summer are associated with transient eddies propagating from northern Tharsis toward the polar cap instead of zonally coherent waves (Tyler and Barnes, 2005).

3.2. Longitude–latitude distribution

Fig. 3 shows the spatial distribution of spring and summer frontal events. Data for all years (Mars Years 24–28) are included in the figure. The patterns for different years are consistent. The mean latitude of these events moves closer to the pole from spring to summer, reflecting the retreat of the north polar cap. Frontal events occur at all longitudes around the polar cap, but there is

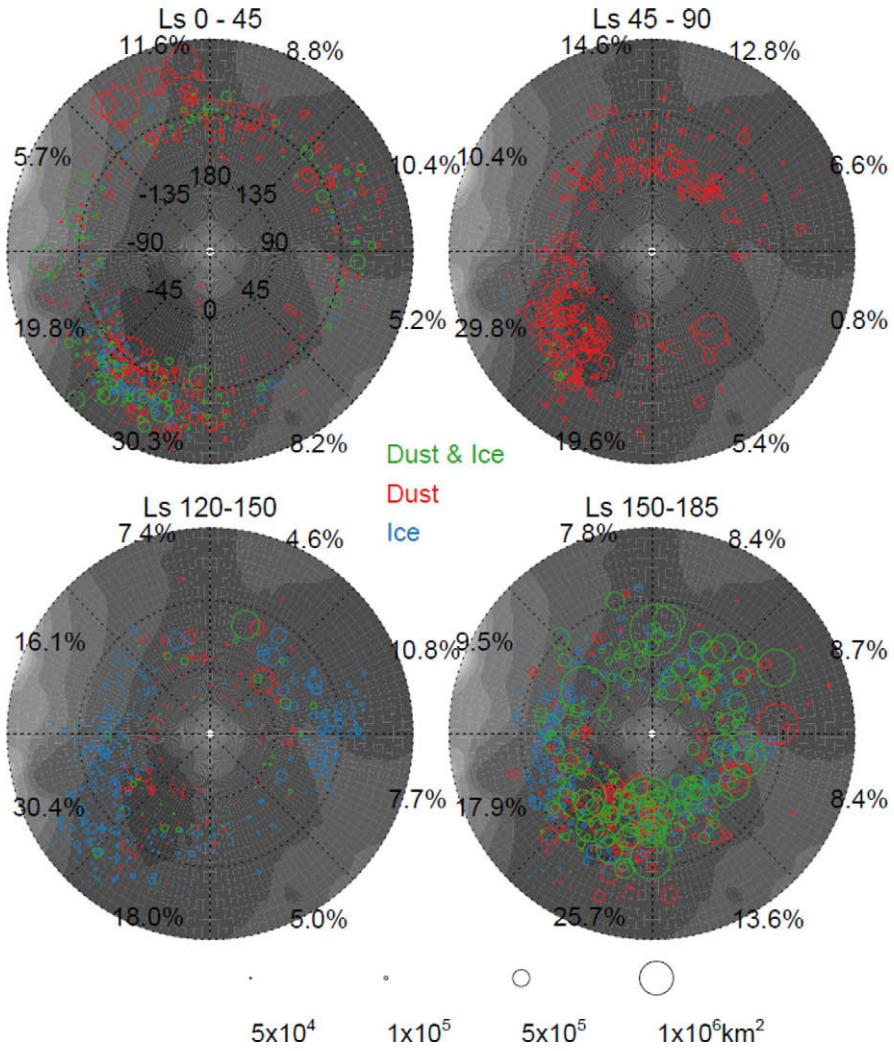

Fig. 3. Spatial distribution of frontal events (red – dust, blue – ice, green – dust and ice) during L_s 0–45° (upper right), L_s 45–90° (upper right), L_s 120–150° (lower left) and L_s 150–185° (lower right). The dotted lines show latitudes 45°, 60°, and 75° and every 45° of longitude. East longitudes are labeled in the upper left panel along the 75°N latitude circle. Topography is plotted as background shadings (dark: low, bright: high) in each panel to provide orientation. The sizes of the symbols are proportional to the areas of the events. Note that the longitude–latitude extent of the symbols does not correspond to those of the observed storms. Events smaller than 5×10^4 km^2 are plotted using the smallest symbol in the legend. The percentage of the number of events in each 45° longitude sector (with respect to the total number of events in the panel) is labeled along the 45°N circle. (For interpretation of the references to color in this figure legend, the reader is referred to the web version of this article.)

an apparent preference for low topography, indicating the presence of storm zones (regions of enhanced eddies). About half of the frontal events are concentrated in the 0–90°W quadrant (especially in the low topography region northeast of Tempe Fossae). Less than 15% are observed in the 0–90°E quadrant (north of Arabia) before L_s 150°. In late summer, features generally have larger size and longer lifetimes. Many can therefore travel long distances with the dominant eastward winds in this season, smearing the longitudinal distributions. For instance, the percentage of events in the 0–45°E sector is only 5–8% before L_s 150° but increases to about 14% during L_s 150–180°. TES data also show a preference for higher dust opacities in the 0–90°W quadrant in late spring (Tamppari et al., 2008).

The cluster of relatively large (>5×10^5 km^2) events in the 0–90°W sector is centered on 30°W during L_s 0–45°, 45°W during L_s 45–90° and 15°W during L_s 150–185°. GCM simulations show that the strongest meridional wind variance is centered to the northeast of Tempe Fossae in early spring and late summer and shifts westward to the area north of Alba Patera (~110°W) in mid-spring (Hollingsworth et al., 1997). The direction of the shift in the model is consistent with the results in Fig. 3; however, the sector with the most frontal events is always east of the longitude of Alba Patera in MDGM observations.

TES temperatures at 6.1 hPa for Mars Years 24–25 show that the strongest transient variations are in the 0–60°E sector (north of Arabia) and the 60–120°W sector (north of Tempe Terra and Alba Patera) in early spring and in the 0–120°E sector in late summer (Banfield et al., 2004). These sectors are upstream of the most populated sectors in Fig. 3. Several factors can result in the disagreement: (1) Fig. 3 tends to emphasize the downstream region since a frontal event may have traveled some distance before being captured in an image and a long-lived event is recorded multiple times (once per day) in the downstream region; (2) A well developed spiral such as that shown in Fig. 1m shows very little temperature anomaly since the air has been mixed; (3) Tracers (dust storms/ice clouds) are not always present to highlight the flow; (4) Since 6.1 hPa is about 5 km (roughly half an atmospheric scale height) above the surface in the north polar region, thermal signatures of shallower systems do not contribute to variations at this level. Tyler and Barnes (2005) simulated a jet streak (maximum winds in the jet stream) on the zonal jet north of Alba Patera for L_s 150°. The region north of Acidalia is at the left exit region of this jet

streak where the associated secondary circulation can induce baroclinic storms. This is consistent with the results in Fig. 3. Tyler and Barnes (2005) showed an example where the simulated location of the strongest temperature variability (in the longitude sector between Elysium and Alba Patera) was different from that of the strongest wind variability (northeast of Tempe Fossae), implying that the eddy heat flux pattern was different from the eddy momentum flux pattern. The storm zone position therefore depends on the meteorological fields being considered. For Mars Year 26, in addition to the sectors mentioned above, there is enhanced TES 6.1 hPa temperature variability in the 0–45°W sector (north of Acidalia) where most of the frontal events are observed.

Arc-shaped clouds north of Tharsis (in the 45–135°W sector) first appear after the early summer (i.e. solstitial) hiatus in the frontal event distribution. Tyler and Barnes (2005) suggested that they were related to transient eddies propagating from Tharsis toward the polar cap edge. Their Fig. 9 showed two separate routes – one from Alba Patera and the other from Tempe Fossae – in excellent agreement with MDGM observations. Clouds in the 45–180°E sector occur about a month later than arc clouds north of Tharsis. They are usually transformed from cloud patches to front-like morphology by atmospheric circulation.

3.3. Complex events

Many frontal events in spring and summer show complex morphologies (Section 2.1) indicating complex circulations. The distributions of complex events (other than simple fronts and arcs) are shown as purple circles in Fig. 4. In the temporal distribution (top panel), about a quarter of the observed frontal events are complex for L_s 30–60° and L_s 150–180°, and only about 10% for L_s 0–30° and L_s 120–150°. In the spatial distribution (bottom panel), about a quarter are complex in the 0–90°W sector, 18% in the 0–45°E sector, and about 10% in other sectors, suggesting topographic effects.

A case study combing MOC and TES data is performed for a complex frontal event at $L_s \sim$ 162–163° of Mars Year 24 (Fig. 5). This event was captured in five consecutive MOC images during the first sol and four consecutive images on the second sol. It first appeared as an upside-down comma in MDGM involving both dust and ice and developed into the first regional spiral in late summer of the year (Cantor et al., 2001; Wang and Ingersoll, 2002). Winds derived from cloud tracking (using all available images for this event) show cyclonic rotation and northeastward translation. TES temperature perturbations are derived by subtracting a base temperature, which is defined by a linear fit of the temperatures within 100 TES orbits, 30° longitude, and 1° latitude of the current orbit as a function of time (data are gridded with 1° latitude bins). Temperature perturbations at 6.1 hPa show that the comma arm (75–80°N) is at the boundary between northern cold air and southern warm air (upper left panel). Warm air is being wrapped into the center of the forming spiral and moving northward, consistent with the presence of the cloud band north of the dust arm (upper left panel). Cold air is present behind the comma and moving eastward (upper right panel). The distinct thermal signature decreases with altitude (lower right panel). It is lost by 2.88 mb and flips sign at higher levels. Traveling waves in TES temperatures are derived using the least squares method of Wu et al. (1995) with a sliding window of 16 sols (for 6–8 sol waves), 12 sols (for 4–6 sol waves) or eight sols (for 2–4 sol waves). Eastward traveling waves at 6.1 hPa (70.5–73°N, lower left panel) are usually coherent for more than a week. The dominant wave modes transition from 4-sol Wave 1 before L_s 158° to 2-sol Wave 3 (and 8-sol Wave 1) during L_s 160–165° and to 4-sol Wave 2 after L_s 165°. This is similar to the wave mode transition seen in MGS radio science data (Hinson, 2006; Hinson and Wang, in preparation). The L_s 162–163° frontal event in Fig. 5 occurred when the amplitude of 2–3 sol Wave 3 maximized along with that of 8-sol Wave 1. A 5-sol Wave 2 mode was also noticeable during this period. After L_s 165°, MDGM shows apparent Wave 2 manifested by two large eastward traveling frontal events on opposite sides of the polar cap (Wang and Ingersoll, 2002).

A second case study for the event at L_s 152–154° of Mars Year 26 is shown in Fig. 6. This event was among the first regional spi-

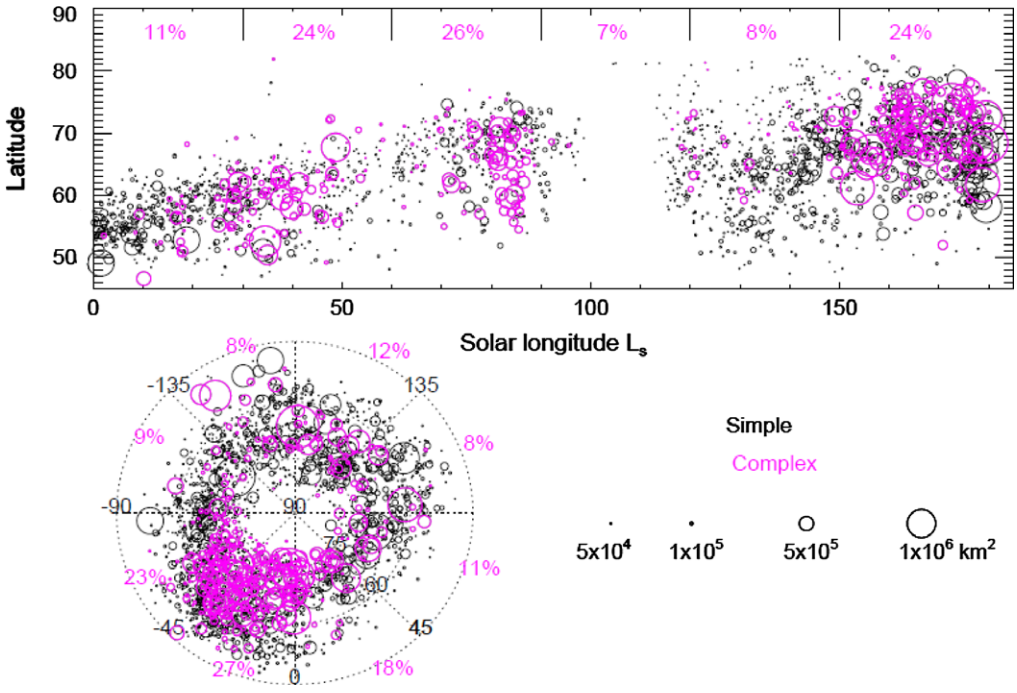

Fig. 4. (Top) L_s–latitude and (bottom) longitude–latitude distribution of simple (black, including simple fronts and arcs) and complex (purple, including all the other morphologies) frontal events. Each panel includes data for northern springs and summers of Mars Years 24–28. Symbols are plotted as described in Figs. 2 and 3. (For interpretation of the references to color in this figure legend, the reader is referred to the web version of this article.)

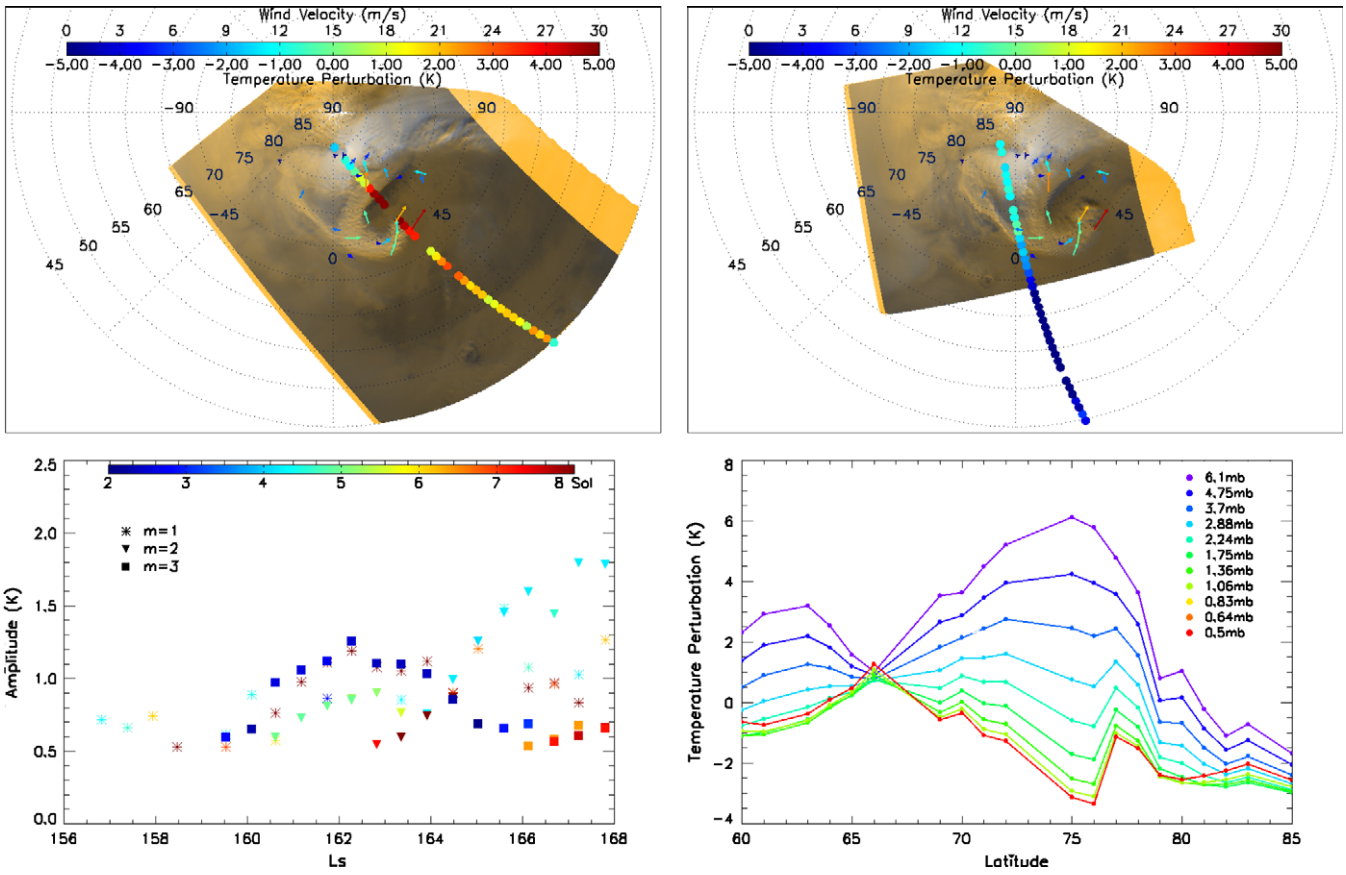

Fig. 5. Case study for the L_s 162–163° event of Mars Year 24. Cloud-tracked winds and TES temperature perturbations at 6.1 hPa are superimposed on projected MOC images (upper left) m0204734 and (upper right) m0204742. The images are 2 h apart. The lower left panel shows the amplitudes of dominant eastward traveling waves with zonal wave number of 1 (star), 2 (triangle) and 3 (square) as a function of L_s for 70.5–73°N. Colors indicate the periods of the corresponding waves. The lower right panel shows TES temperature perturbations along the track associated with m0204734 in the upper left panel as a function of latitude for different levels indicated by different colors. (For interpretation of the references to color in this figure legend, the reader is referred to the web version of this article.)

rals in late summer of the year and lasted for four sols. Cloud-tracked winds indicate cyclonic rotation and southeastward translation. Temperature perturbations at 6.1 hPa show that the northern arm of the spiral was located on the cold–warm air boundary and the eye of the spiral was characterized by a warm temperature anomaly (upper left panel). This distinct temperature signature again decreases with altitude and is confined below 2.88 mb (lower right panel). Temperature anomalies at higher levels indicate warm air above the spiral. In contrast to the event in Fig. 5, the spiral in this case was mainly located in warm air at low levels (upper right panel). The event occurred during an interval when eastward traveling Wave $m = 1$ (7–8 sol) were dominant with secondary Wave $m = 3$ (2–3 sol, lower left panel). Wave mode transitions between 4–5-sol Wave $m = 3$ and 6–8-sol Wave $m = 1$ occurred at $L_s \sim 148°$ and 158° during the period.

While both our examples show a direct correspondence between MOC and TES observations, there are also cases when substantial temperature anomalies are not associated with any dust storms/clouds and cases when frontal events are not associated with any temperature anomalies. Statistics of which frontal event in MOC images posesses a corresponding temperature signature in TES data awaits further study.

3.4. Travel trajectories

Fig. 7 summarizes the general travel paths of the observed frontal events during L_s 0–60°, 60–120°, and 120–180° (all years included). The paths are based on impressions of cloud/dust storm motions obtained from animated MDGM instead of tracked winds as used in Wang and Ingersoll (2003). They qualitatively indicate the general wind directions with respect to the polar cap.

During L_s 0–60°, frontal events travel eastward around the polar cap edge, consistent with the dominant wind directions predicted by TES thermal wind balance and numerical models (e.g., James et al., 1999; Banfield et al., 2003). They sometimes travel towards or away from the polar cap in low topography longitude sectors north of Acidalia, Arcadia and Utopia. Model results show these regions to be storm zones with strong transient wind variability (Hollingsworth et al., 1997). Similarly, frontal events during L_s 120–180° also travel eastward around the polar cap. Occasionally, they travel towards the cap in the longitude sector north of Acidalia and Arabia, and away from the cap in the longitude sector north of Utopia. At the beginning of this time period, a few events in the sector north of Acidalia travel westward at the cap edge and turn eastward at lower latitudes. They probably reflect the transition of circulation from summer-like to winter-like conditions.

The L_s 60–120° period is more complicated – there are westward paths at the cap edge and eastward paths at most longitudes further south. Note the travel paths do not reflect near-surface circulation during the early summer hiatus period due to the lack of clouds and dust storms. Mesoscale simulations show both retrograde (westward) and prograde (eastward) storm progression in late spring when the circulation is in transition and sensitive to the polar cap extent and atmospheric dust opacity (Tyler et al., 2008). Fig. 5 shows southward paths in the longitude sector of Acidalia. Many relatively large dust storms in late spring follow this southward path and dissipate within the same longitude sector. Tyler et al. (2008) simulated storms with little zonal motion and

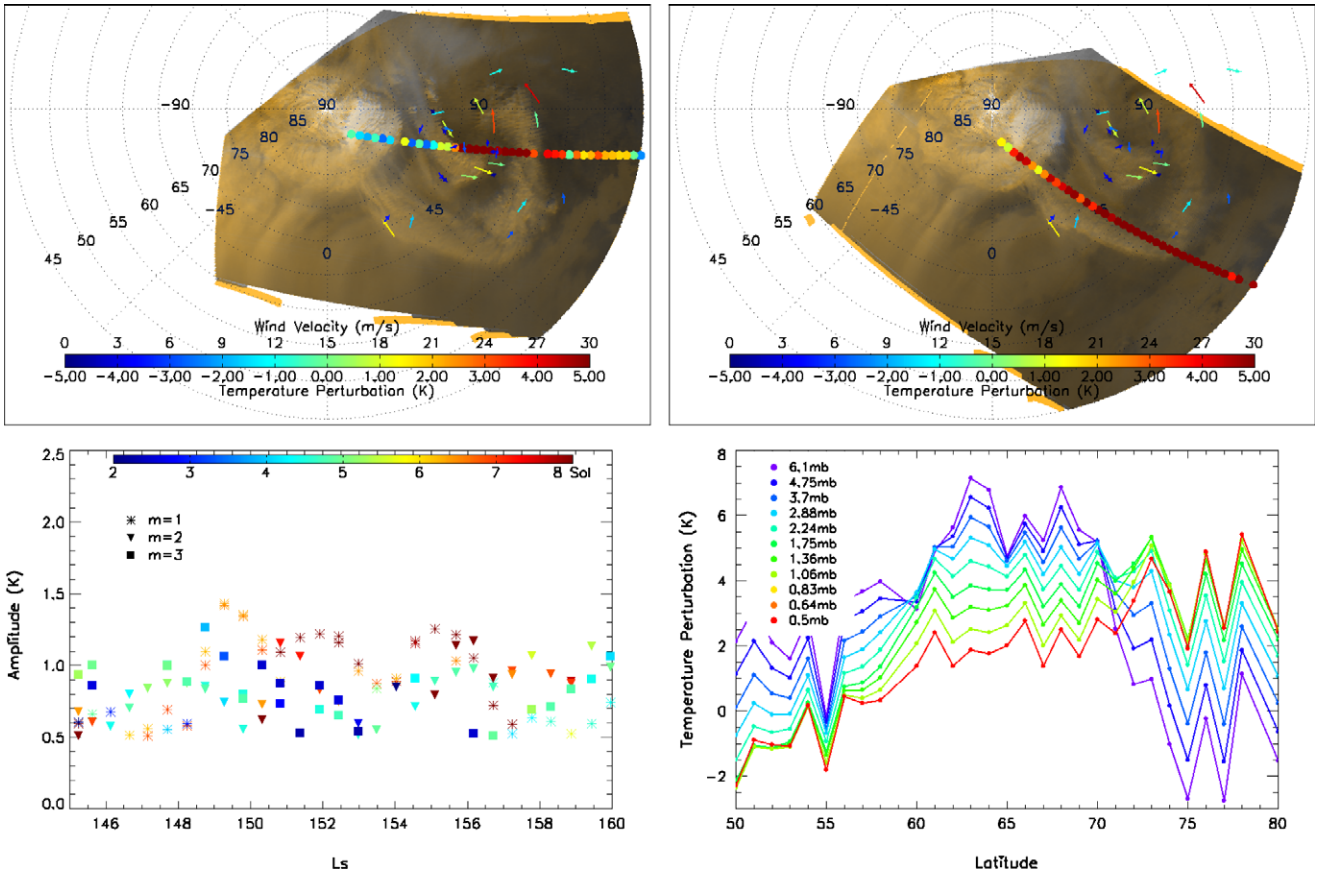

Fig. 6. Case study for the L_s 152–154° event of Mars Year 26. Cloud-tracked winds and TES temperature perturbations at 6.1 hPa are superimposed on projected MOC images (upper left) r0300792 and (upper right) r0300794. The images are 2 h apart. The lower left panel shows the amplitudes of dominant eastward traveling waves with zonal wave number of 1 (star), 2 (triangle) and 3 (square) as a function of L_s for 65–67.5°N. Colors indicate the periods of the corresponding waves. The lower right panel shows TES temperature perturbations along the track associated with r0300792 in the upper left panel as a function of latitude for different levels indicated by different colors. (For interpretation of the references to color in this figure legend, the reader is referred to the web version of this article.)

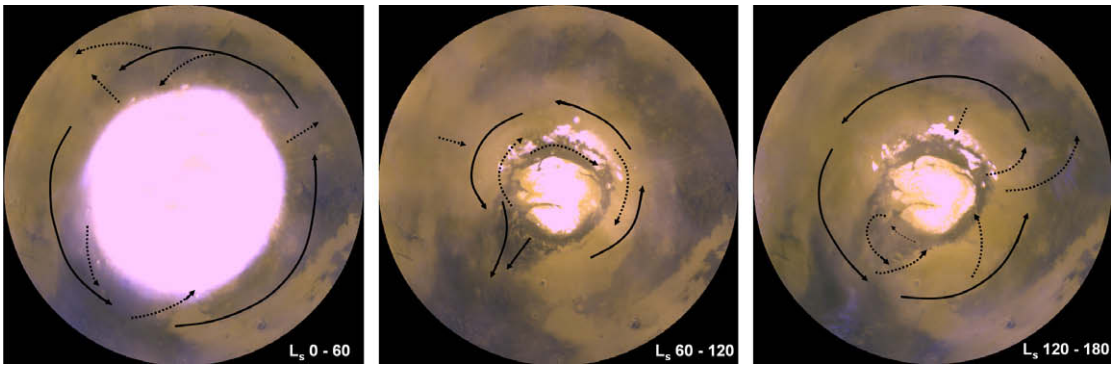

Fig. 7. Paths of frontal events derived from MDGM animations for L_s 0–60°, 60–120°, and 120–180°. Solid arrows indicate main paths. Dotted arrows indicate occasional paths. Arrows lengths and latitudinal positions are arbitrary. All available northern spring and summer MDGM (from Mars Year 24 to Mars Year 28) are considered in making this figure.

described complex wavenumber transitions in late spring. Abundant water vapor exists in the atmosphere during this period due to the exposure of the north polar residual cap (Smith, 2002, 2008), and Acidalia may be an important path through which water vapor is transported to lower latitudes.

4. Summary and discussion

The complete archive of MGS MOC Mars Daily Global Maps (Mars Years 24–28, 1999–2006) is used to study north polar (45–90°N) frontal clouds and dust storms during spring and summer (L_s 0–180°), complementing previous studies for fall and winter (L_s 180–360°) (Wang et al., 2003, 2005; Wang, 2007).

The observed frontal events range from local to regional scale in dust storm classification and are influenced by local to planetary scale circulations. They exhibit a wide variety of morphologies suggestive of complex flow patterns. Early afternoon clouds and dust storms are absent in MDGM in early summer, leading to a gap in the seasonal distribution of frontal events. In agreement with our observations, TES temperatures and radio science geopotential heights show much weaker transient eddies in early summer than

those in the rest of the year (Banfield et al., 2003, 2004; Hinson, 2006). Travel paths of clouds and dust storms indicate dominant westward (easterly) winds at the edge of the polar cap near summer solstice. Numerical models indicate near-surface easterlies in the vicinity of the polar cap for this time period, which inhibit the vertical propagation of planetary waves (Tyler and Barnes, 2005; Basu et al., 2006). The general atmospheric conditions in early spring and late summer are winter-like, with a westerly jet and planetary waves. Frontal events in these periods are probably related to dynamical instability of the zonal flow. Under summer-like conditions with cap edge easterlies, frontal events (as we call them) are expected to be influenced more by local and regional circulation.

TES shows high 2PM dust opacities in early summer (Tamppari et al., 2008) when MOC shows no apparent dust storms (on the early afternoon side). We speculate that this is probably due to the presence of dust devil or small scale circulation sustained haze that is hard to recognize in images. The amount of water vapor maximizes in early summer, but clouds are rare (at least in early afternoon) (Smith, 2002, 2008). The atmosphere attains high water vapor holding capacity due to warm temperatures (relative to the frost point) (Richardson et al., 2002). Weak eddies during this period will likely limit water vapor transport to lower latitudes.

Frontal events are observed at all longitudes, however, low topography areas, especially northeast of Tempe Fossae, are apparently favored. This region is downwind of the strongest storm zones derived from TES temperatures in Mars Year 24 (Banfield et al., 2004), but shows enhanced temperature variations in Mars Year 26. In late summer, frontal events travel eastward with the intensifying polar jet, contributing additional counts to the adjacent 0–45° longitudinal sector. The definition of the most prominent martian storm zones appears to be sensitive to the variables and altitudes chosen. Frontal storms may preferentially form within the regions of strong baroclinicity and continue to develop as they travel downstream.

Case studies show that distinct temperature signatures at lower levels closely correspond to features observed in images. Temperature perturbations at upper levels do not provide as direct a link as those at lower levels, but the upper level circulation may play a role in the development of cyclones and fronts. Each case has its own particular course of development. Collectively, frontal events are important for dust, ice and water vapor exchange between the high and low latitudes. Expressions of frontal events by dust/ice do not always occur concurrently with sharp changes in temperature and other meteorology fields due to lack of visible tracers, shallowness of the system, or mixing of air masses. This can result in disagreement between conclusions drawn from MOC and TES. There are apparent transitions in the dominant wave modes in TES temperatures in early spring and late summer. Transitions at upper levels may involve fewer modes since those with wave numbers higher than two are confined to the lower atmosphere.

About 70% of the frontal events in mid-summer are ice clouds north of Tharsis and Utopia. Those north of Tharsis (specifically Alba Patera and Tempe Fossae) are characterized by arc shapes. Some arcs can develop spiral features. Model results suggest that arc-shaped clouds are related to transient eddies propagating from Alba Patera and Tempe Fossae toward the north polar cap (Tyler and Barnes, 2005). Clouds north of Utopia usually appear first as patches (with fluffy structure suggestive of shallow convection). They are sometimes transformed by the ambient flow to adopt a front-like morphology.

Long-term systematic daily global observations are crucial for studying martian weather and climate. Mars Reconnaissance Orbiter (MRO) has continued daily global mapping of Mars after MGS. Similar analyses with MRO data are needed to better understand the climatology and variability of martian clouds and dust storms and to improve our understanding of martian atmospheric circulation through modeling. Results presented in this paper can be used to evaluate model performance in terms of the composition, sizes, timing, locations and paths of frontal events. Models can in turn help explain the underlying dynamics, assess the momentum, energy and tracer transport capacity, and test sensitivity to dust haze and topography.

Acknowledgments

This study is supported by NASA Mars Data Analysis program. We thank Daniel Tyler Jr. for providing comments on improving our manuscript. We thank R. John Wilson and Mark I. Richardson for their thoughtful reviews.

References

Albee, A., 2002. The Mars Global Surveyor mission: Description, status, and significant results. Highlights Astron. 12 (12), 631–635.
Balme, M., Greeley, R., 2006. Dust devils on earth and mars. Reviews of Geophysics 44 (3), RG3003. doi:10.1029/2005RG000188.
Banfield, D., Conrath, B.J., Gierasch, P.J., Wilson, R.J., Smith, M.D., 2004. Traveling waves in the martian atmosphere from MGS TES Nadir data. Icarus 170, 365–403.
Banfield, D., Conrath, B.J., Smith, M.D., Christensen, P.R., Wilson, R.J., 2003. Forced waves in the martian atmosphere from MGS TES nadir data. Icarus 161, 319–345.
Barnes, J.R., 1980. Time spectral analysis of midlatitude disturbances in the martian atmosphere. J. Atmos. Sci. 38, 225–234.
Barnes, J.R., 1981. Mid-latitude disturbances in the martian atmosphere – A 2nd Mars year. J. Atmos. Sci. 38, 225–234.
Barnes, J.R., Pollack, J.B., Haberle, R.M., Leovy, C.B., Zurek, R.W., Lee, H., Schaeffer, J., 1993. Mars atmospheric dynamics as simulated by the NASA Ames general-circulation model. 2. Transient baroclinic eddies. J. Geophys. Res. Planets 98, 3125–3148.
Basu, S., Richardson, M.I., Wilson, R.J., 2004. Simulation of the martian dust cycle with the GFDL mars GCME. J. Geophys. Res. Planets 109, E11006. doi:10.1029/2004JE002243.
Basu, S., Wilson, R.J., Richardson, M.I., Ingersoll, A.P., 2006. Simulation of spontaneous and variable global dust storms with the GFDL Mars GCM. J. Geophys. Res. Planets 111, E09004. doi:10.1029/2005JE002660.
Benson, J.L., Bonev, B.P., James, P.B., Shan, K.J., Cantor, B.A., Caplinger, M.A., 2003. The seasonal behavior of water ice clouds in the Tharsis and Valles Marineris regions of Mars: Mars Orbiter Camera observations. Icarus 165, 34–52.
Benson, J.L., James, P.B., Cantor, B.A., Remigio, R., 2006. Interannual variability of water ice clouds over major martian volcanoes observed by MOC. Icarus 184, 365–371.
Cantor, B.A., 2007. MOC observations of the 2001 Mars planet-encircling dust storm. Icarus 186, 60–96.
Cantor, B., Malin, M., Edgett, K.S., 2002. Multiyear Mars Orbiter Camera (MOC) observations of repeated martian weather phenomena during the northern summer season. J. Geophys. Res. Planets 107, E35014. doi:10.1029/2001JE001588.
Cantor, B.A., James, P.B., Caplinger, M., Wolff, M.J., 2001. Martian dust storms: 1999 Mars Orbiter Camera observations. J. Geophys. Res. Planets 106, 23653–23687.
Christensen, P.R., and 10 colleagues, 1992. Thermal emission spectrometer experiment – Mars-observer mission J. Geophys. Res. Planets 97, 7719–7734.
Clancy, R.T., Sandor, B.J., Wolff, M.J., Christensen, P.R., Smith, M.D., Pearl, J.C., Conrath, B.J., Wilson, R.J., 2000. An intercomparison of ground-based millimeter, MGS TES, and Viking atmospheric temperature measurements: Seasonal and interannual variability of temperatures and dust loading in the global Mars atmosphere. J. Geophys. Res. Planets 105, 9553–9571.
Fisher, J.A., Richardson, M.I., Newman, C.E., Szwast, M.A., Graf, C., Basu, S., Ewald, S.P., Toigo, A.D., Wilson, R.J., 2005. A survey of martian dust devil activity using Mars Global Surveyor Mars Orbiter Camera images. J. Geophys. Res. Planets 110, E03004. doi:10.1029/2003JE002165.
Greeley, R., Balme, M.R., Iversen, J.D., Metzger, S., Mickelson, R., Phoreman, J., White, B., 2003. Martian dust devils: Laboratory simulations of particle threshold. J. Geophys. Res. Planets 108 (E5), 5041. doi:10.1029/2002JE001987.
Hinson, D.P., 2006. Radio occultation measurements of transient eddies in the northern hemisphere of Mars. J. Geophys. Res. Planets 111, E05002. doi:10.1029/2005JE002612.
Hinson, D.P., Wilson, R.J., 2004. Temperature inversions, thermal tides, and water ice clouds in the martian tropics. J. Geophys. Res. Planets 109, E01002. doi:10.1029/2003JE002129.
Hollingsworth, J.L., Haberle, R.M., Schaeffer, J., 1997. Seasonal variaions of storm zones on Mars Planetary Atmospheres and Ionospheres and Reference Atmospheres, Adv. Space Res. 19 (8), 1237–1240.
Holton, J.R., 1992. An Introduction to Dynamic Meteorology. Academic Press.
Houze Jr., R.A., 1994. Cloud Dynamics. Academic Press.

James, P.B., Hollingsworth, J.L., Wolff, M.J., Lee, S.W., 1999. North polar dust storms in early spring on Mars. Icarus 138, 64–73.
Kauhanen, J., Siili, T., Jarvenoja, S., Savijarvi, H., 2008. The Mars limited area model and simulations of atmospheric circulations for the Phoenix landing area and season of operation. J. Geophys. Res. Planets 113, E00A14. doi:10.1029/2007JE003011.
Kuroda, T., Medvedev, A.S., Hartogh, P., Takahashi, M., 2007. Seasonal changes of the baroclinic wave activity in the northern hemisphere of Mars simulated with a GCM. Geosphys. Res. Lett. 34 (9), L09203. doi:10.1029/2006GL028816.
Malin, M.C., Danielson, G.E., Ingersoll, A.P., Masursky, H., Veverka, J., Ravine, M.A., Soulanille, T.A., 1992. Mars-Observer Camera. J. Geophys. Res. Planets 97, 7699–7718.
Montmessin, F., Forget, F., Rannou, P., Cabane, M., Haberle, R.M., 2004. Origin and role of water ice clouds in the Martian water cycle as inferred from a general circulation model. Journal of Geophysical Research-Planets. 109 (E10), E10004. doi:10.1029/2004JE002284.
Newman, C.E., Lewis, S.R., Read, P.L., Forget, F., 2002a. Modeling the martian dust cycle – 1. Representations of dust transport processes. J. Geophys. Res. Planets 107 (E12), 5123. doi:10.1029/2002JE001910.
Newman, C.E., Lewis, S.R., Read, P.L., Forget, F., 2002b. Modeling the martian dust cycle – 2. Multiannual radiatively active dust transport simulations. J. Geophys. Res. Planets 107 (E12), 5124. doi:10.1029/2002JE001920.
Pearl, J.C., Smith, M.D., Conrath, B.J., Banfield, J.L., Christensen, P.R., 2001. Observations of martian ice clouds by the Mars Global Surveyor thermal emission spectrometer: The first martian year. J. Geophys. Res. Planets 106, 12325–12338.
Rafkin, S.C.R., Maria, M.R.V.S., Michaels, T.I., 2002. Simulation of the atmospheric thermal circulation of a martian volcano using a mesoscale numerical model. Nature 419, 697–699.
Richardson, M.I., Wilson, R.J., Rodin, A.V., 2002. Water ice clouds in the martian atmosphere: General circulation model experiments with a simple cloud scheme. J. Geophys. Res. Planets 107 (E9), 5064. doi:10.1029/2001JE001804.
Rodin, A.V., Wilson, R.J., 2006. Seasonal cycle of martian climate: Experimental data and numerical simulation. Cosmic Res. 44, 329–333.
Smith, M.D., 2002. The annual cycle of water vapor on Mars as observed by the thermal emission spectrometer. J. Geophys. Res. Planets 107 (E11), 5115. doi:10.1029/2001JE001522.
Smith, M.D., 2004. Interannual variability in TES atmospheric observations of Mars during 1999–2003. Icarus 167, 148–165.
Smith, M.D., 2008. Spacecraft observations of the martian atmosphere. Ann. Rev. Earth Planetary Sci. 36, 191–219.
Tamppari, L.K., Amith, M.D., Bass, D.S., Hale, A.S., 2008. Water–ice clouds and dust in the north polar region of Mars using MGS TES data. Planetary Space Sci. 56, 227–245.
Toigo, A.D., Richardson, M.I., Wilson, R.J., Wang, H., Ingersoll, A.P., 2002. A first look at dust lifting and dust storms near the south pole of Mars with a mesoscale model. J. Geophys. Res. Planets 107, E75050. doi:10.1029/2001JE001592.
Tyler, D., Barnes, J.R., 2005. A mesoscale model study of summertime atmospheric circulations in the north polar region of Mars. J. Geophys. Res. Planets 110, E06007. doi:10.1029/2004JE002356.
Tyler, D., Barnes, J.R., Skyllingstad, E.D., 2008. Mesoscale and large-eddy simulation model studies of the martian atmosphere in support of Phoenix. J. Geophys. Res. Planets. 113, E00A12. doi:10.1029/2007JE003012.
Wang, H.Q., 2007. Dust storms originating in the northern hemisphere during the third mapping year of Mars Global Surveyor. Icarus 189, 325–343.
Wang, H.Q., Ingersoll, A.P., 2002. Martian clouds observed by Mars Global Surveyor Mars Orbiter Camera. J. Geophys. Res. Planets 107 (E10), 5078. doi:10.1029/2001JE001815.
Wang, H.Q., Ingersoll, A.P., 2003. Cloud-tracked winds for the first Mars Global Surveyor mapping year. J. Geophys. Res. Planets 108 (E9), 5110. doi:10.1029/3002JE002107.
Wang, H.Q., Richardson, M.I., Wilson, R.J., Ingersoll, A.P., Toigo, A.D., Zurek, R.W., 2003. Cyclones, tides, and the origin of a cross-equatorial dust storm on Mars. Geophys. Res. Lett. 30 (E9), 1488. doi:10.1029/2002GL016828.
Wang, H.Q., Zurek, R.W., Richardson, M.I., 2005. Relationship between frontal dust storms and transient eddy activity in the northern hemisphere of Mars as observed by Mars Global Surveyor. J. Geophys. Res. Planets 110, E07005. doi:10.1029/2005JE002423.
Whelley, P.L., Greeley, R., 2008. The distribution of dust devil activity on Mars. J. Geophys. Res. Planets 113, E07002. doi:10.1029/2007JE002966.
Wilson, R.J., Hinson, David, Smith, Michael D., 2006. GCM simulations of transient eddies and frontal systems in the martian atmosphere. Second Workshop on Mars Atmosphere: Modeling and Observations. CNES-ESA, Granada, Spain.
Wu, D.L., Hays, P.B., Skinner, W.R., 1995. A Least-squares method for spectral analysis of space–time series. J. Atmos. Sci. 52, 3501–3511.
Zurek, R.W., Martin, L.J., 1993. Interannual variability of planet-encircling dust storms on Mars. J. Geophys. Res. Planets 98 (E2), 3247–3259.